EASR

Engineering and Applied Science Research

https://www.tci-thaijo.org/index.php/easr/index

Published by the Faculty of Engineering, Khon Kaen University, Thailand

Effect of aspect ratios on stress and strain of a multilayer model for the left ventricle

Prapatsorn Sangpin*, Phrut Sakulchangsatjatai, Niti Kammuang-lue and Pradit Terdtoon

Department of Mechanical Engineering, Faculty of Engineering, Chiang Mai University, Chiang Mai 50200, Thailand

Received 19 September 2017
Accepted 16 January 2018

Abstract

A basic understanding of the heart behavior assists in the accurate diagnosis of heart disease, which is the leading cause of death in Thailand. The mechanical behaviors of the heart can be ideally explained by strain and stress. This work numerically and analytically described three layers of the heart wall in a computational model, while previous studies only considered the myocardium, which is a muscular layer. Moreover, the shape of the left ventricle (LV) varies among individuals. The influence of the LV shape, as assumed to be a truncated ellipse, was considered by varying the short-to-long-axis and wall-to-cavity-volume ratios to investigate strain and stress in the radial, circumferential and longitudinal directions during a passive filling with blood using a continuum approach. For verification, the model was compared to other research work by defining the wall-to-cavity-volume and short-to-long-axis ratios as well by as fiber distribution. The results showed that an increasing short-to-long-axis ratio obviously resulted in decreased overall strains and stresses. Whereas, increasing the wall-to-cavity-volume ratio slightly decreased radial contraction as well as circumferential and longitudinal expansion. The fiber strains of the linear fiber distribution corresponded well with previous work at a high longitudinal curvature.

Keywords: Computational model, Endocardium, Epicardium, Left-ventricular shape, Stress, Strain

1. Introduction

Cardiovascular disease (CVD) was the leading cause of death of Thai people in 2012 [1] and more than 58,000 of Thais will die annually from this disease [2]. However, it is preventable and mostly treatable with early detection. A computational model of the left ventricle (LV) or the left chamber of the heart that pumps blood through the whole body is used to understand heart behavior. Its analysis will give support as a tool for medical diagnosis in case of CVDs. Several computational models of the LV have been presented assuming the shape as a cylinder [3-4], a truncated cone [5-6], and truncated ellipse [7-8]. Most focused on the myocardium, which is a muscular layer responding for the heart function. The heart is composed of three layers, endocardium, myocardium, and epicardium located at the inner, middle and outer wall, respectively [9]. The endocardium and epicardium are extremely thinner than the myocardium, but they are capable of carrying loads in the circumferential and longitudinal direction [10-11]. They show isotropic behavior, but exhibit a highly nonlinear behavior near the limit of extensibility and have a major influence in a passive filling process [12]. Hence, the one-layer LV model is inadequate. Moreover, the LV size and shape is different among individuals based upon gender, age, and health, resulting in different stress and strain values. CVDs caused remodeling in the LV shape so that the chamber was more spherical and the LV wall increased [13-14]. The various LV shapes also lead to changes in fiber angles, which is influent in a twisting deformation and cardiac function [15]. Individuals with a high sphericity in the LV shape are at high risk of heart failure as well as atrial fibrillation [16]. Even though there were previous studies concerned about the influence of LV shape, they only considered the myocardium in their models [7, 17]. In the current study, an analytical method using a continuum approach was applied to determine strain and stress in a multi-layer model. Then strain and stress were compared for various LV shapes in terms of short-to-long-axis and wall-to-cavity-volume ratios during the passive filling phase.

2. Methodology

2.1 Left ventricular model

The LV geometry was assumed to be a truncated ellipse in a prolate spheroidal coordinate system (X_1, X_2, X_3) that provided a good correlation with the actual LV shape 0. The X_1 coordinate varies along the radial direction perpendicular to the confocal LV surface, whereas the X_2 and X_3 coordinates provide the circumferential and longitudinal position on the surface, respectively, as seen in Figure 1(a). The transformation between prolate spheroidal and Cartesian (X, Y, Z) coordinates is given by 0:

$$\begin{aligned} X &= d \cdot \sinh(X_1)\cos(X_2)\sin(X_3) \\ Y &= d \cdot \sinh(X_1)\sin(X_2)\sin(X_3) \\ Z &= d \cdot \cosh(X_1)\cos(X_3) \end{aligned} \quad (1)$$

*Corresponding author.
Email address: sangpin.p@gmail.com
doi: 10.14456/easr.2018.40

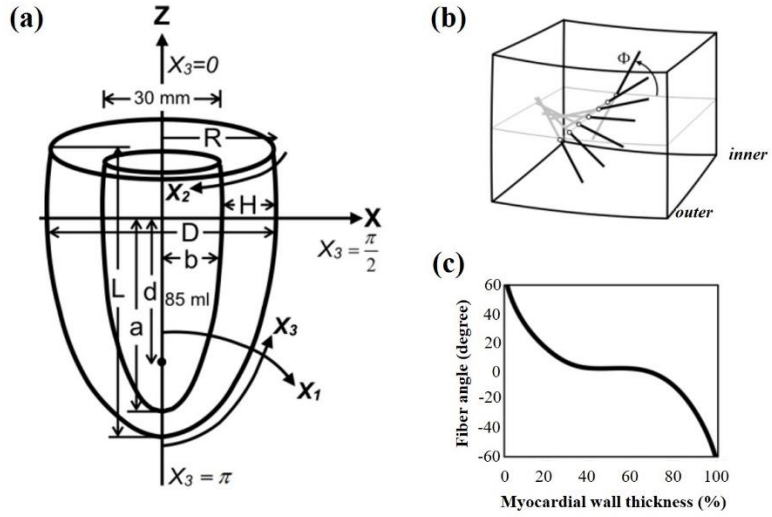

Figure 1 (a) Parameters are illustrated in the prolate spheroidal coordinate system. (b) The distribution of the fiber angles in the myocardium is defined. (c) The fiber angle helically distributes 60° and -60° at the inner and outer surface, respectively.

where the focal length (d) is given by $d = \sqrt{a^2 - b^2}$, a and b are the major and minor radii of the ellipsoid, respectively, as shown in Figure 1(a).

The initial cavity volume was 85 ml, and the final volume of blood filled into the LV chamber during a passive filling was 100 ml [7]. The basal diameter of the LV shape was fixed at 30 mm [8] representing the mitral valve annulus in Figure 1(a).

The LV shape was defined by the short-to-long-axis and wall-to-cavity-volume ratios, which were controlled parameters for all various shapes. The short-to-long-axis ratio is the ratio between the minor (b) and major (a) radii of the ellipsoid, while the wall-to-cavity-volume ratio is the ratio between the volume of LV cavity and wall.

2.2 Myocardium

The myocardium is a muscular layer composed of helical fibers, which are oriented spirally and smoothly across the wall 0 as shown in Figure 1(b). The helical angle (Φ) of the nonlinear fiber distribution in the myocardium is shown in Figure 1(c) and is defined by:

$$\Phi(\mathrm{R}) = \Phi(R_i) - \left\{1 + \left[\frac{2R-(R_o+R_i)}{R_o-R_i}\right]^3\right\}\left(\frac{\Phi(R_i)-\Phi(R_o)}{2}\right) \quad (2)$$

where R_i and R_o are undeformed inner and outer radii, respectively, measured from X_1=0. The deformation gradient (F_{ij}) of the myocardium can be written as:

$$F_{ij} = \begin{bmatrix} \partial r/\partial R & \partial r/R\partial\Theta & \partial r/\partial Z \\ r\partial\theta/\partial R & r\partial\theta/R\partial\Theta & r\partial\theta/\partial Z \\ \partial z/\partial R & \partial z/R\partial\Theta & \partial z/\partial Z \end{bmatrix} = \begin{bmatrix} r' & 0 & 0 \\ r\omega' & r/R & r\psi \\ w' & 0 & \Lambda \end{bmatrix} \quad (3)$$

where ψ is a twist-per-unit undeformed length, ω and w are a radially dependent part of the circumferential and apex-to-base displacement, respectively, and Λ is an extension ratio in the apex-to-base direction.

Using the right Cauchy-Green deformation tensor ($C = F^T \cdot F$), the components of the Green strain (E_{ij}) calculated by $E = (C - I)/2$ are:

$$E_{11} = [(r')^2 + (r\omega')^2 + (w')^2 - 1]/2 \quad (4a)$$

$$E_{22} = [(r/R)^2 - 1]/2 \quad (4b)$$

$$E_{33} = [(r\psi)^2 + (\Lambda)^2 - 1]/2 \quad (4c)$$

The first principal strain invariant (I_1) is:

$$I_1 = tr\boldsymbol{C} = (r')^2 + (r\omega')^2 + (r/R)^2 + (r\psi)^2 + (w')^2 + (\Lambda)^2 \quad (5)$$

The stretch ratio in the fiber direction (α) is derived by a unit vector in the fiber direction in undeformed LV ($\boldsymbol{N}$), which is: $\alpha^2 = \boldsymbol{N} \cdot \boldsymbol{C} \cdot \boldsymbol{N}^T$.

$$N_i = [0, \cos\Phi(\mathrm{R}), \sin\Phi(\mathrm{R})] \quad (6)$$

$$\alpha^2 = \{(r/R)^2\cos^2\Phi(\mathrm{R}) + 2(r/R)(\mathrm{r}\psi)\sin\Phi(\mathrm{R})\cos\Phi(\mathrm{R}) + [(\mathrm{r}\psi)^2 + (\Lambda)^2]\sin^2\Phi(\mathrm{R})\} \quad (7)$$

The constitutive relation, which describes the mechanical behavior of the myocardium, was expressed as a strain-energy function, (W). It was derived in terms of the first strain invariant (I_1) and stretch ratio in the fiber direction (α) as [4]:

$$W = A\left[e^{a(I_1-3)} - 1\right] + B\left[e^{b(\alpha-1)^2} - 1\right] \quad (8)$$

where A, a, B and b are material parameters derived from multi-axial test. The main components of the Cauchy stress (σ_{ij}) for the myocardium are:

$$\sigma_{11} = -p(r) + 2W_I(r')^2 \quad (9a)$$

$$\sigma_{22} = -p(r) + 2W_I[(r/R)^2 + (r\psi)^2 + (r\omega')^2] + (W_\alpha/\alpha)[\alpha^2 - (\Lambda^2\sin^2\Phi(\mathrm{R})] \quad (9b)$$

$$\sigma_{33} = -p(r) + 2W_I[(w')^2 + (\Lambda)^2] + (W_\alpha/\alpha)[\Lambda^2\sin^2\Phi(\mathrm{R})] \quad (9c)$$

where $p(r)$ is the Lagrange multiplier for incompressibility, $W_I = aAe^{a(I_1-3)}$ and $W_\alpha = 2b(\alpha-1)Be^{b(\alpha-1)^2}$ are partial differentiations of the constitutive relation expressed in Equation 8 on I_1 and α, respectively.

Table 1 Material parameters of the endocardium and epicardium

	Endocardium		Epicardium	
Direction	**Circumferential**	**Longitudinal**	**Circumferential**	**Longitudinal**
c (g/cm)	7.58 x 10^{-4}	3.82 x 10^{-4}	2.94 x 10^{-3}	2.94 x 10^{-4}
c_1	6.66	5.93	0.78	0.78
c_2	12.8	12.1	12.9	9.69
c_3	6.36	6.32	0.20	0.20
c_4 (g/cm)	2.94	0.20		
c_5 (g/cm)	2.94	0.20		
c_6 (g/cm)	0.20	4.60		

$$p(r) = 2W_I(r')^2 + P_i - \int_{r_i}^{r} \frac{1}{r}\left\{\begin{matrix} 2W_I[(r/R)^2 + (r\psi)^2 + (r\omega')^2 - (r')^2] \\ +(W_\alpha/\alpha)[\alpha^2 - \Lambda^2 \sin^2\Phi(\mathrm{R})] \end{matrix}\right\} dr. \quad (10)$$

2.3 Endocardium and epicardium

The endocardial and epicardial layers are extremely thin that could be conducted under a biaxial test in the circumferential and apex-to-base direction [10-11]. Then, the in-plane shear stresses of these layers are zero and the deformation gradient tensor is:

$$F_{ij} = \begin{bmatrix} \lambda_R & 0 & 0 \\ 0 & \lambda_\Theta & \kappa_\Theta \\ 0 & \kappa_Z & \lambda_Z \end{bmatrix} \quad (11)$$

where λ_i is the stretch ratio and κ_i is shear value that cannot be controlled and should not exceed 0.2 0. The right Cauchy-Green deformation tensor was used to calculate the Green strain.

The behaviors of the endocardium and epicardium were similar, but the endocardium was stiffer at lower extensions [10-11]. The constitutive relation for the endocardium was described by a combined polynomial-exponential pseudostrain-energy function 0:

$$Q = 0.5c_1E_{\Theta\Theta}^2 + c_2E_{\Theta\Theta}E_{ZZ} + 0.5c_3E_{ZZ}^2 \quad (12)$$

$$W = c(e^Q - 1) + 0.5c_4E_{\Theta\Theta}^2 + c_5E_{\Theta\Theta}E_{ZZ} + 0.5c_6E_{ZZ}^2 \quad (13)$$

The equation for the epicardium was a Fung-type exponential pseudostrain-energy function:

$$W = c(e^Q - 1) \quad (14)$$

where c and c_i are material parameters. The membrane stresses ($\boldsymbol{t}$ in gf/cm) in the circumferential and longitudinal directions of the endocardium and epicardium were directly determined from the constitutive equations ($t = \frac{1}{J} \cdot F \cdot \frac{\partial W}{\partial E} \cdot F^T$) 0. The equilibrium equation providing the Lagrange multiplier was used to calculate the radial stress. The details of strain and stress calculation were provided in a previous study 0.

2.4 Boundary conditions

The border between layers were attached in the circumferential and longitudinal directions. The circumferential and longitudinal deformations at the border between the endocardium and myocardium were equal ($E_{22}(R_{o,endo}) = E_{22}(R_{i,myo})$ and $E_{33}(R_{o,endo}) = E_{33}(R_{i,myo})$) and vice versa between the myocardium and epicardium ($E_{22}(R_{o,myo}) = E_{22}(R_{i,epi})$ and $E_{33}(R_{o,myo}) = E_{33}(R_{i,epi})$). The circumferential deformation showed that the undeformed and deformed radii at the border were equal and κ_Z was zero. The longitudinal strain between layers was used to determine κ_Θ. Moreover, the transmural pressure, which perpendicularly acts to the heart wall, resulted in radial stress and was even between layers ($\sigma_{11}(r_{o,endo}) = \sigma_{11}(r_{i,myo})$ and $\sigma_{11}(r_{o,myo}) = \sigma_{11}(r_{i,epi})$).

2.5 Parameters

A short-to-long-axis ratio was constant during passive filling with settings of 0.5 to 0.99, and the wall-to-cavity-volume ratios were set to 1, 2 and 3. The initial and final cavity volume was constrained at 85 and 100 ml [7], respectively, for all LV shapes. The basal diameter representing the heart valve position was assumed to be 30 mm, as seen in Figure 1(a), through the filling process [7-8]. The outer pressure (P_0) was constant at 0 kPa [7-8].

The material parameters for the myocardium were as follows [4]: ψ = 1.7/cm, A = 0.115 kPa, a = 9.665, B = 0.082 kPa, b = 61.52, $w'(R_i)$ = 0.2, and $\omega'(R_i)$ = 0.1 rad/cm. The fiber angle varied from 60° at inner wall to -60° at outer wall [6].

The wall thickness of the endocardium and epicardium was 0.188 and 0.297 mm, respectively 0. The material parameters obtained by using a nonlinear curve-fitting method of the extracted data from the biaxial test (circumferential and longitudinal direction) on six animals 0 are shown in Table 1 for the endocardium and epicardium.

3. Results

3.1 Strains and stresses

The overview of strains and stresses are given in Figures 2 and 3, respectively, in three main directions, radial (X_1), circumferential (X_2), and longitudinal (X_3) direction, and in the right half of a longitudinal cross-section. A deformed LV is in front of an undeformed LV drawn in a black line.

During passive filling, the LV expanded in the longitudinal and circumferential directions, especially at the apex, as seen in Figures 2(c) and 2(b), respectively. The circumferential and longitudinal expansion was consistent with observations of the heart during blood filling 0. According to the incompressibility of the heart wall, the LV radially contracted particularly at the apex in Figure 2(a). The circumferential and longitudinal deformation decreased from the inner wall to the outer wall as well as the radial contraction.

The stress distributions in the radial, circumferential and longitudinal direction are shown in Figure 3. During blood filling, the deformation mostly took place at the apex and

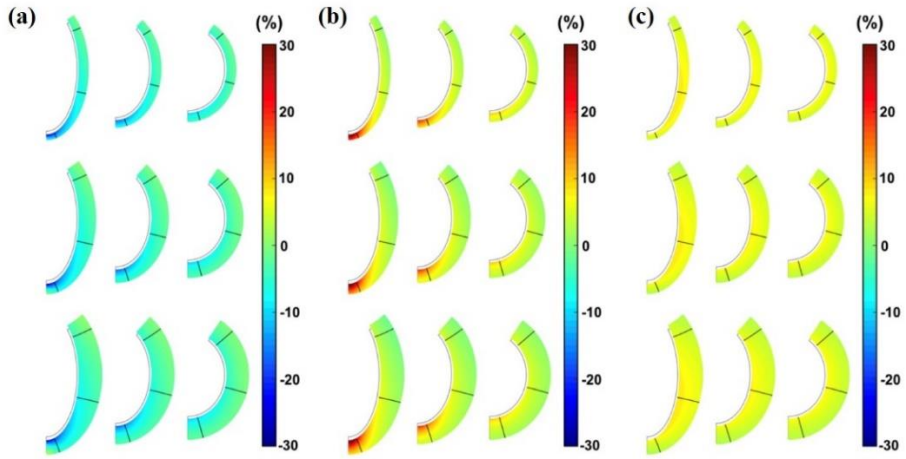

Figure 2 Strain distributions in (a) radial, (b) circumferential and (c) longitudinal direction. The distributions are shown for short-to-long-axis ratios of 0.5, 0.7, and 0.9 from left to right, and for wall-to-cavity-volume ratios of 1, 2 and 3 from the top to bottom.

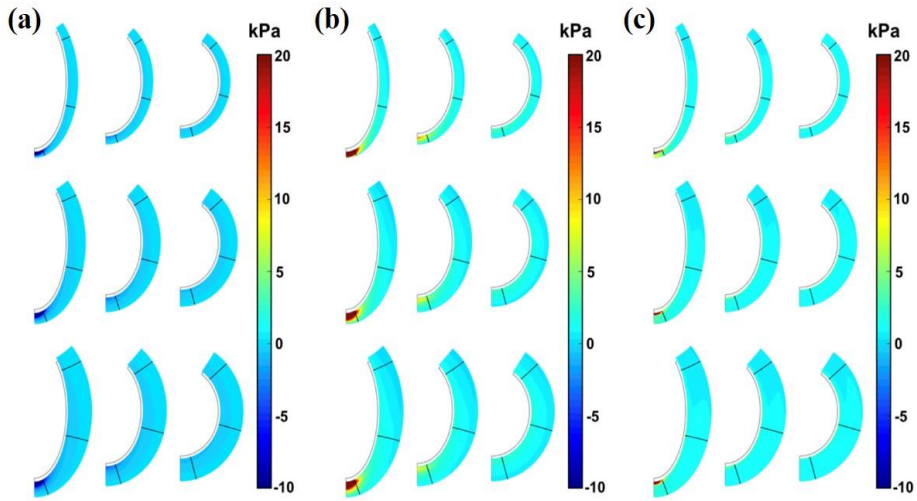

Figure 3 Stress distributions in (a) radial, (b) circumferential and (c) longitudinal direction. The distributions are shown for short-to-long-axis ratios of 0.5, 0.7, and 0.9 from left to right, and for wall-to-cavity-volume ratios of 1, 2 and 3 from the top to bottom.

caused maximum stress at the apex. The magnitude of stress in all directions was high at the inner wall and then gradually decreased to the outer wall.

Increasing the short-to-long-axis ratios obviously decreased the strain and stress in all directions. Increasing the wall-to-cavity-volume ratios insignificantly varied both contraction and expansion.

The middle wall of each layer was selected to observe variation in the short-to-long-axis ratio. The three longitudinal positions were measured at 10%, 50% and 90% from the base of an undeformed LV, represented as the base, mid-LV, and apex, respectively, as indicated by the black lines in Figures 2-3.

In Figure 4(a), the endocardium was more radially contracted than other two layers. With an increasing short-to-long-axis ratio or increasing degree of sphericity, the contraction in all layers was gradually increased at the base, but it significantly decreased in contraction at the apex. The endocardium had the highest circumferential and longitudinal expansion. The circumferential expansion in Figure 4(b) slightly increased at the base, insignificantly varied at the mid-LV, but extremely decreased at the apex for increasing short-to-long-axis ratios. As seen in Figure 4(c), the longitudinal expansion of the base slightly varied in the myocardium and epicardium, while it increased in the endocardium. All layers tended to decrease in longitudinal deformation at the mid-LV and slightly changed at the apex during an incremental change in sphericity.

With increasing longitudinal curvature, the stress in the epicardium was insignificantly different at the base, mid-LV, and apex in all directions. The radial stress, as seen in Figure 5(a), in the endocardium at the apex was greatly high for low longitudinal curvature in LV shape according to the transmural pressure acting at the wall surface while the apex extremely contracted in the radial direction. At the apex, the circumferential and longitudinal stress, in Figure 5(b) and 5(c), respectively, in the endocardium increased and then insignificantly decreased. The stress in the circumferential and longitudinal directions in the myocardium were substantially higher for a low sphericity LV shape and then decreased with high sphericity. A nonlinear fiber distribution in the myocardium resulted in high circumferential stress, especially for the low short-to-long-axis ratio.

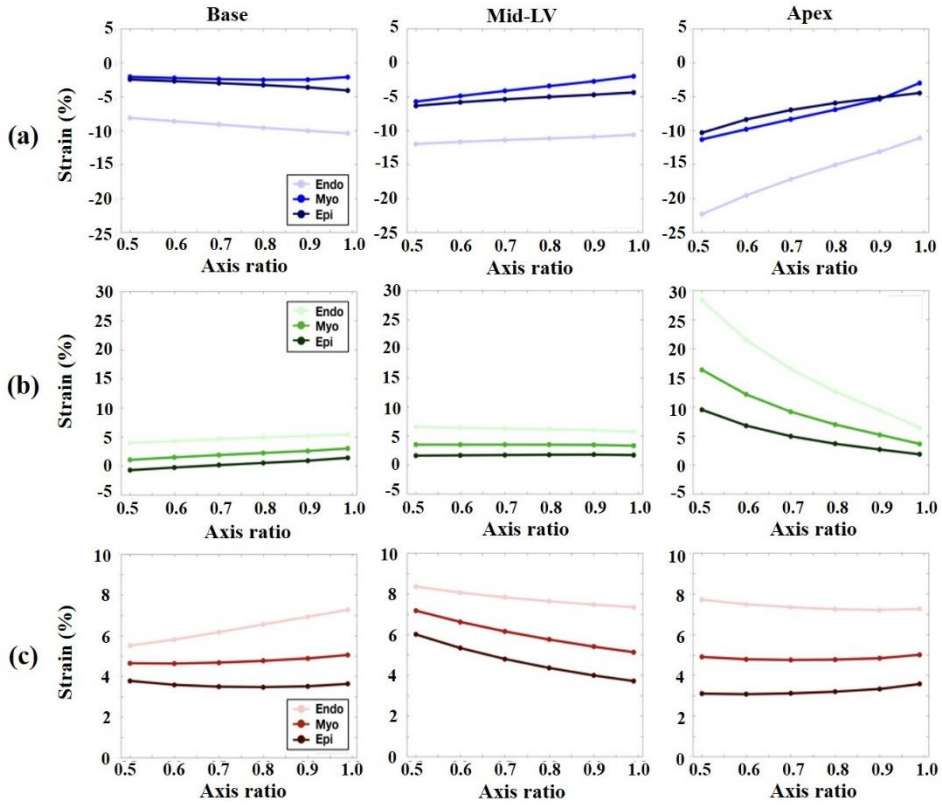

Figure 4 Strain distribution at the middle layer of the endocardium, myocardium and epicardium for wall-to-cavity-volume ratios of 2 and short-to-long-axis ratios of 0.5, 0.6, 0.7, 0.8, 0.9 and 0.99 at the base, mid-LV, and apex from left to right as indicated by black lines in Figure 2 in (a) radial, (b) circumferential, and (c) longitudinal directions.

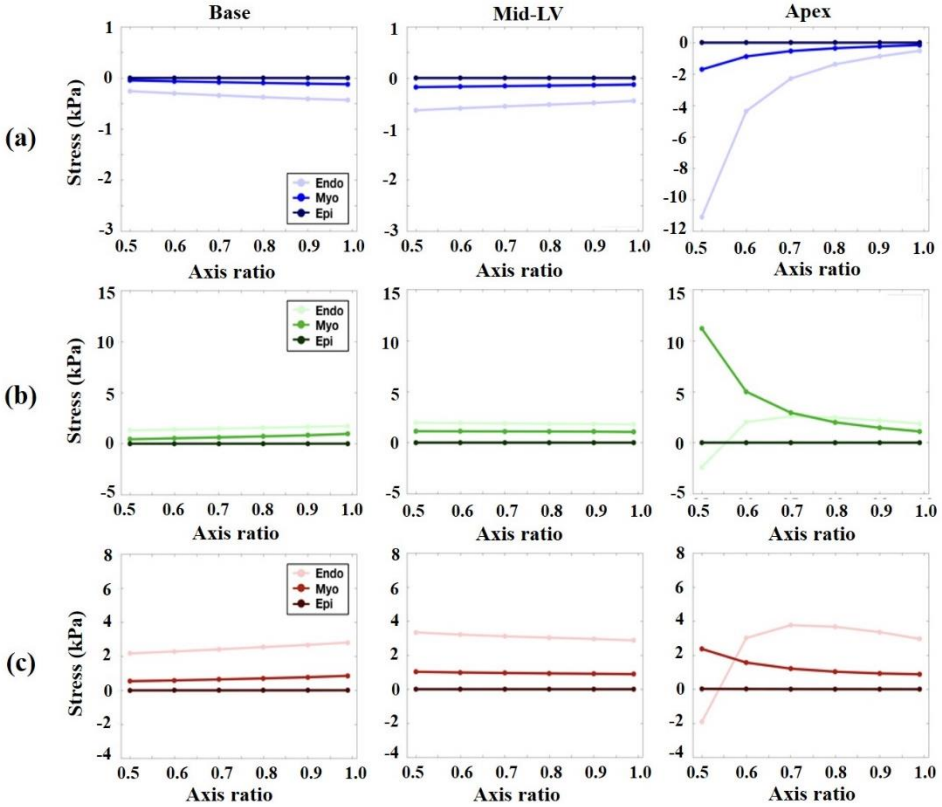

Figure 5 Stress distribution at the middle layer of the endocardium, myocardium and epicardium for wall-to-cavity-volume ratios of 2 and short-to-long-axis ratios of 0.5, 0.6, 0.7, 0.8, 0.9 and 0.99 at the base, mid-LV, and apex from left to right as indicated by black lines in Figure 3 in (a) radial, (b) circumferential, and (c) longitudinal directions.

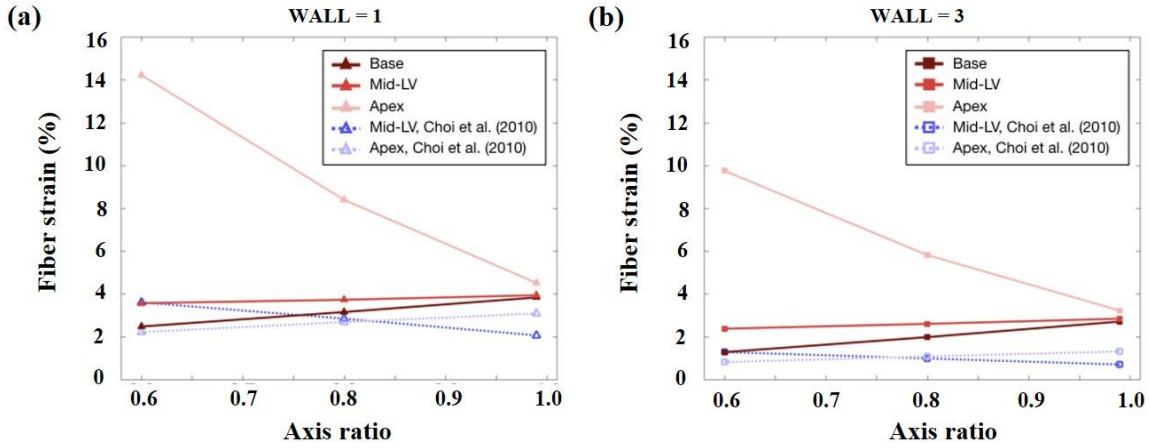

Figure 6 Distribution of fiber strain in short-to-long-axis ratios of 0.6, 0.8 and 0.99 at the base, mid-LV, and the apex of linear fiber distribution at the middle myocardium, in comparison to Choi et al. (2010) [7].

3.2 Model verification

For verification, the model was compared to other with respect to fiber direction since they only considered the myocardium layer. The fiber direction depends on the circumferential and longitudinal direction and was simply determined using strain transformation. Parameters were varied to match Choi et al. (2010) [7] in that the fiber distribution was linear and aligned 75° to -45° at inner and outer walls, respectively. The twist-per-unit undeformed length was zero ($\psi = 0$), the wall-to-cavity-volume ratios were 1 and 3, short-to-long-axis ratio were 0.6, 0.8 and 0.99. Figure 6 shows fiber strains for wall-to-cavity-volume ratios of 1 and 3 at mid-LV (equator line or Z = 0) and apex.

The strain in the fiber direction for the wall-to-cavity-volume ratio of 1 in Figure 6(a) was rather higher than the wall-to-cavity-volume ratio of 3 in Figure 6(b). Increasing the short-to-long-axis ratio showed that the fiber strain increased at the base and mid-LV, while it certainly decreased at the apex. At high short-to-long-axis ratios (axis ratio > 0.8), the fiber strain at the apex was higher than other longitudinal positions, which is consistent with other, even though the magnitude was different.

4. Discussion

Increasing the wall-to-cavity-volume ratio presented a small variation of strains by reducing radial contraction as well as decreasing circumferential and longitudinal expansion and stress. This occurred while increasing radial stress and decreasing stress in the circumferential and longitudinal direction. Whereas increasing the short-to-long-axis ratio or longitudinal curvature of LV shape showed a wide variation of strains and stresses, especially at the apex, as seen in Figures 4 and 5, respectively.

Considering the fiber direction, increasing the wall-to-cavity-volume ratio showed that the fiber strain decreased while increasing the short-to-long-axis ratio certainly caused strain reduction in the fiber direction at the apex. The more that the LV shape is spherical, the less the LV circumferentially expands, which can easily be seen in Figure 4(b) at the apex. This is because the high spheroidal shape of LV evenly dissipates load during LV expansion. The fiber strain with high longitudinal curvature was similar to that reported by Choi et al. (2010) [7] that the strain at the apex was higher than at the mid-LV for wall-to-cavity-volume ratios of 1 and 3, even though the magnitude was different. Thus, the model was appropriate for investigation of strain and stress of the three LV layers.

Even though a truncated ellipse is close to the actual LV shape, an imaging technique such as a magnetic resonance imaging (MRI) or a computed tomography (CT) scan will give real geometry and other parameters such as a cavity pressure, LV size, and thickness. Moreover, a lack of validation in the same specimen or animal was seen in the discontinuous distribution of stain and stress across the three layers of the LV wall in some directions. To complete the multi-layer model for the LV, the material parameters should be determined on the same animal or specimen.

Factors such as tissue growth, remodeling, and acute geometric change could alter residual stress. These can be observed in the ratio of wall thickness to radius and opening angle of the LV sliced ring 0. Dilated cardiomyopathy resulted in a decreaced ratio of wall thickness to radius, and may cause a major decrease in residual strain and stress 0. Considering a cardiac disease condition, residual stress should be significantly considered in the model because it plays a major role in acute geometric remodeling from reduction surgery of a dilated heart. This type of remodeling can restore some of the lost residual stress.

In future work, the strain and stress distribution across the three layers of the LV during a passive filling will provide a basic foundation to develop an artificial heart that it should be able to carry higher loads during a cardiac cycle.

5. Conclusions

The computational results showed that the strain and stress in three main directions that can be summarized as follows:

- When the short-to-long-axis ratio was altered from 0.5 to 0.99, the radial and circumferential strain in all layers at the apex was reduced by more than 50% and 75%, respectively, and stresses in the endocardium varied by more than 75%, 170%, and 250%, in the radial, circumferential and longitudinal directions, respectively.
- Varying wall thickness, which is defined by the wall-to-cavity-volume ratio, slightly affected the strain and stress variation at the same short-to-long-axis ratio.
- High curvature assists to distribute the load in all directions, which results in uniformly distributed longitudinal strain and stress.

- The results show that a person who has low sphericity in the LV shape, appears to have higher strain and stress during blood filling than a person with high wall thickness.
- However, the LV under CVDs remodels that as the shape is more spherical [13], the parameters used for the model, such as an intraventricular pressure and material parameters of the constitutive relation of each layer are needed to model the disease condition and are different than those used in this work.

6. Acknowledgements

This research was supported by the Royal Golden Jubilee Ph.D. Program (RGJ) under the Thailand Research Fund (TRF), grant no. PHD/0259/2551.

7. References

[1] World Health Organization. Noncommunicable diseases and mental health [Internet]. 2014 [cited 2017 August 8]. Available from: http://www.who.int/nmh /countries/tha_en.pdf.

[2] Pantawet N, Chaiwan H. The issue of a campaign on world heart day 2015 [Internet]. Bureau of non communicable diseases [cited 2017 February 25]. Available from: http://www.thaincd.com/document /hot%20news/วันหัวใจโลก%202558.pdf.

[3] Chadwick RS. Mechanics of the left ventricle. Biophys J. 1982;39(3):278-88.

[4] Humphrey JD, Yin FCP. Constitutive relations and finite deformations of passive cardiac tissue II: stress analysis in the left ventricle. Circ Res. 1989;65(3):805-17.

[5] Sangpin P, Sakulchangsatjatai P, Terdtoon P, Kammuang-lue N. Pumping mechanics of the left ventricle based on thick-walled conical shell. Proceedings of the 3rd International Conference on Science, Technology, and Innovation for Sustainable Well-Being (STISWB III); 2011 Aug 12-15; Danang, Viet Nam; 2011. p. 235-41.

[6] Khamdaeng T, Sakulchangsatjatai P, Kammuang-lue N, Danpinid A, Terdtoon P. Stresses and strains analysis in the left ventricular wall with finite deformations. Advanced Structured Materials 2011;14:33-42.

[7] Choi HF, D'hooge J, Rademakers FE, Claus P. Influence of left-ventricular shape on passive filling properties and end-diastolic fiber stress and strain. J Biomech. 2010;43:1745-53.

[8] Choi HF, Frank E, Rademakers E, Claus P. Left-ventricular shape determines intramyocardial mechanical heterogeneity. Am J Physiol Heart Circ Physiol. 2011;301:H2351-61.

[9] Seeley RR, Stephens TD, Tate P. Anatomy & Physiology. 8th ed. New York: McGraw-Hill; 2008.

[10] Humphrey JD, Strumpf RK, Yin FCP. Biaxial mechanical behavior of excised ventricular epicardium. Am J Physiol. 1990;259(1 Pt 2):H101-8.

[11] Kang T, Humphrey JD, Yin FCP. Comparison of biaxial mechanical properties of excised endocardium and epicardium. Am J Physiol. 1996;270(6 Pt 2): H2169-76.

[12] Okamoto RJ, Moulton MJ, Peterson SJ, Li D, Pasque MK, Guccione JM. Epicardial suction: a new approach to mechanical testing of the passive ventricular wall. J Biomech Eng. 2000;122(5):479-87.

[13] Opie LH, Commerford PJ, Gersh BJ, Pfeffer MA. Controversies in ventricular remodeling. Lancet 2006;367(9507):356-67.

[14] Harjai KJ, Edupuganti R, Nunez E, Turgut T, Scott L, Pandian NG. Does left ventricular shape influence clinical outcome in heart failure?. Clin Cardiol. 2000;23:813-9.

[15] van Dalen BM, Kauer F, Vletter WB, Soliman OI. van der Zwaan HB, ten Cate FJ, Geleijnse ML. Influence of cardiac shape on left ventricular twist. J Appl Physiol. 2009;108(1):146-51.

[16] Ambale-Venkatesh B, Yoneyama K, Sharma RK, Ohyama Y, Wu CO, Burke GL, Shea S, Gomes AS, Young AA, Bluemke DA, Lima JAC. Left ventricular shape predicts different types of cardiovascular events in the general population. Heart 2016;103:481-2.

[17] Choi HF, Rademakers FE, Claus P. Left-ventricular shape determines intramyocardial stroke work distribution. In: Metaxas D.N., Axel L, editors. Functional Imaging and Modeling of the Heart (FIMH 2011). Lecture Notes in Computer Science. Berlin: Springer; 2011. p. 401-8.

[18] Adhyapak SM, Parachuri VR. Architecture of the left ventricle: Insights for optimal surgical ventricular restoration. Heart Fail Rev. 2010;15(1):73-83.

[19] Budiman H, Talib J. Prolate spheroidal coordinate: An approximation to modeling of ellipsoidal drops in rotating disc contractor column. J Sci Technol. 2011;3(1):87-95.

[20] Zhukov L, Barr AH. Heart-muscle fiber reconstruction from diffusion tensor MRI. Proc IEEE Visualization 2003;14:597-602.

[21] Humphrey JD, Strumpf RK, Yin FCP. A constitutive theory biomembranes: Application to epicardial mechanics. J Biomech Eng. 1992;114(4):461-6.

[22] Gou Z, Sluys LJ, Constitutive modeling of hyperelastic rubber-like materials. Heron J. 2008;53(3):109-32.

[23] Sangpin P, Sakulchangsatjatai P, Kammuang-lue N, Terdtoon P. Stress and strain of multilayer model for the left ventricle. J Porous Media 2017;20(7):577-90.

[24] Codreanu I, Robson MD, Golding SJ, Jung BS, Clarke K, Holloway CJ. Longitudinally and circumferential directed movements of the left ventricle studies by cardiovascular magnetic resonance phase contrast velocity mapping. J Cardiovasc Magn Reson. 2010;12(1):1-8.

[25] Omens JH, Vaplon SM, Fazeli B, McCulloch AD. Left ventricular geometric remodeling and residual stress in the rat heart. J Biomech Eng, 1998;120:715-9.